Appendix – Table of Contents

Appendix Figure S1

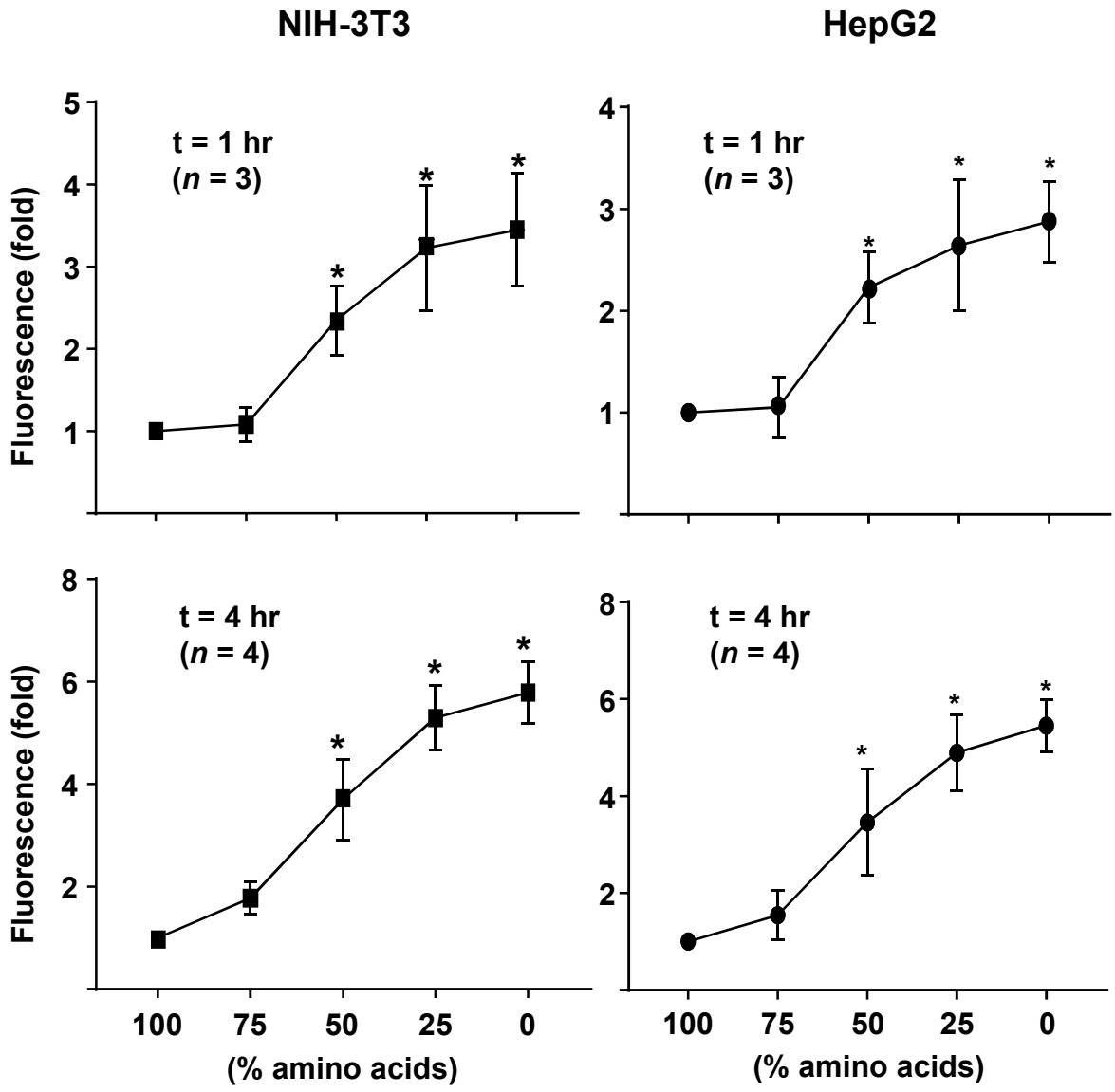

Figure S1. Fluorescence microscopy data showing that AAS increased DiI-LDL uptake in NIH-3T3 and HepG2 cells in a dose-dependent manner. Assays performed at 1 and 4 hr after incubation. Data were expressed as mean ± SD. * $P < 0.05$ versus 100%, one-way ANOVA.

Appendix Figure S2

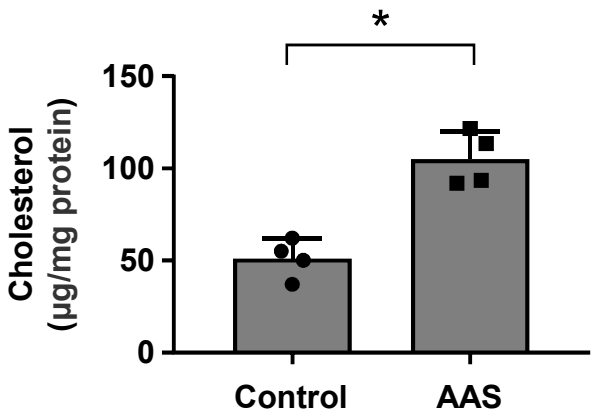

Figure S2. Effect of amino acid starvation (AAS, 50% of the normal level for 60 min) on the cellular cholesterol content in NIH-3T3 cells cultured in the presence of exogenous LDL (50 μg/mL). Data were mean ± SD. * $P < 0.05$, unpaired *t*-test.

Appendix Figure S3

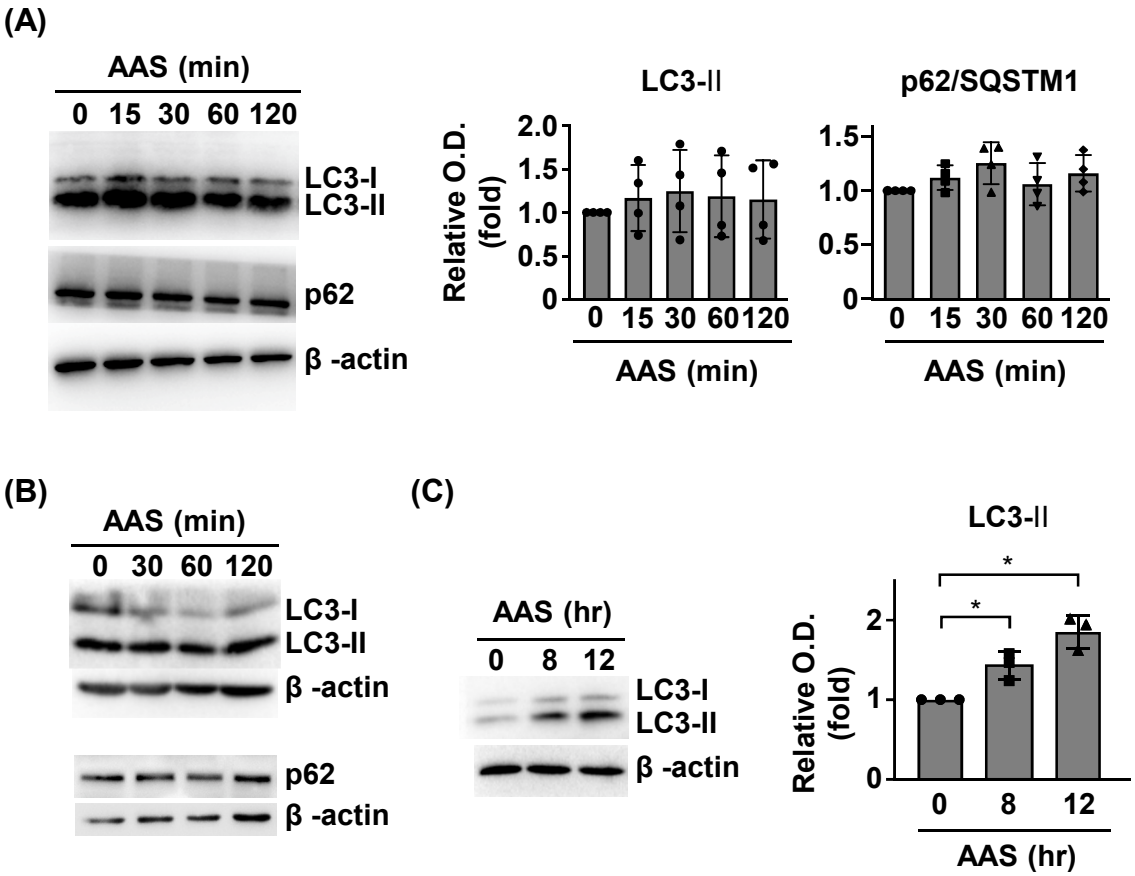

Figure S3. Western blot experiments showing the time course of AAS (50% of normal level) effects on autophagy in (A) HepG2 cells and (B & C) NIH-3T3 cells. Autophagy was assessed by the relative levels of LC3-II and p62/SQSTM1. AAS could not induce autophagy by 2 hr (A & B), but triggered autophagy after treatment for a longer time interval (C). Data were mean ± SD. * $P < 0.05$, one-way ANOVA.

Appendix Figure S4

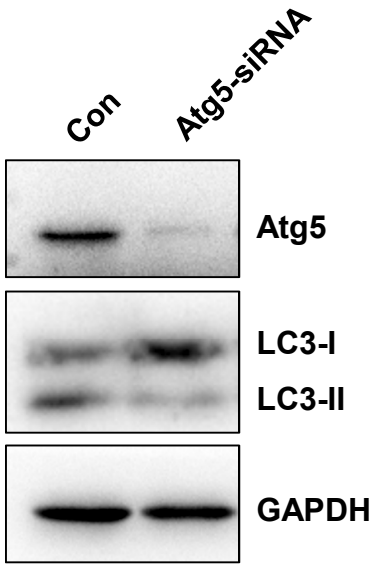

Figure S4. Representative western blots showing that treatment of HepG2 cells with Atg5-siRNA reduced the expression level of Atg5 protein, and attenuated the basal level of autophagy as evidenced by the decrease in LC3-II.

Appendix Figure S5

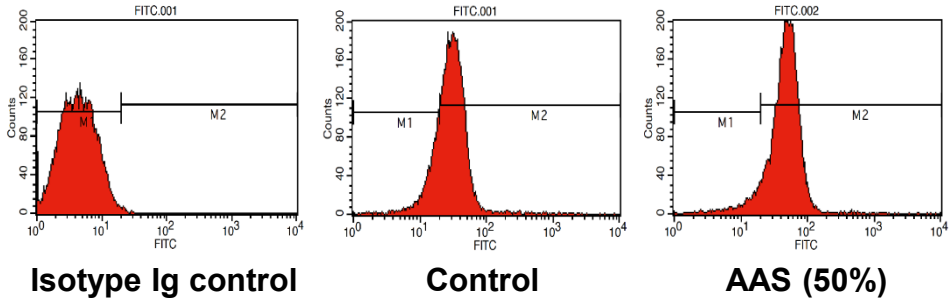

Figure S5. Flow cytometry results showing that AAS increased the abundance of LDLRs on cell surface in non-permeabilized HepG2 cells (example from 3 independent experiments).

Appendix Figure S6 (part 1)

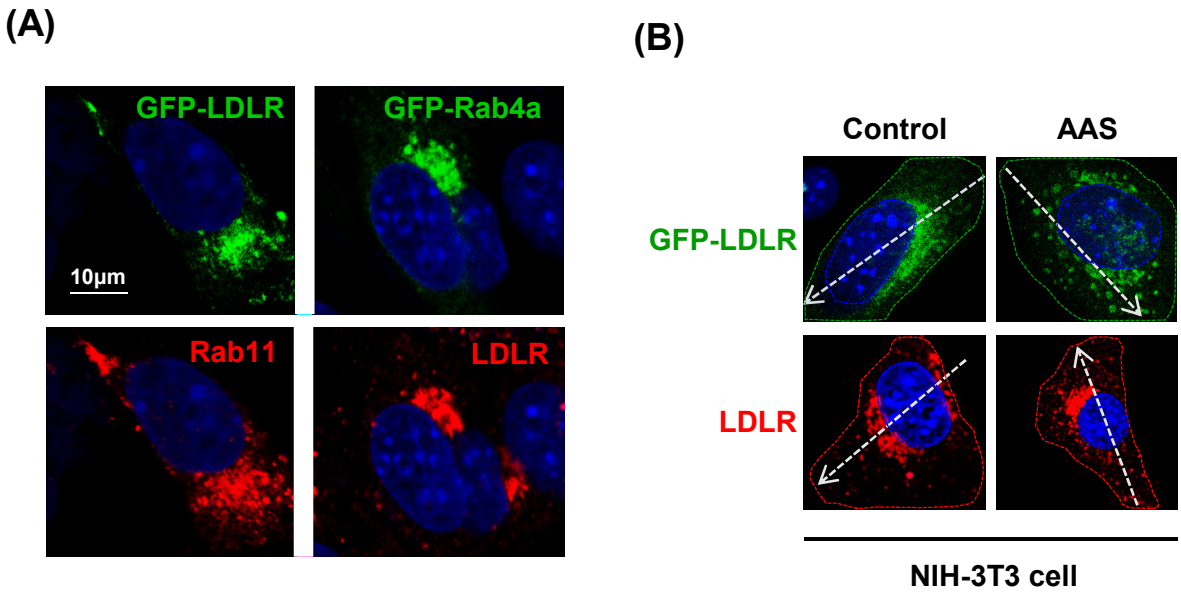

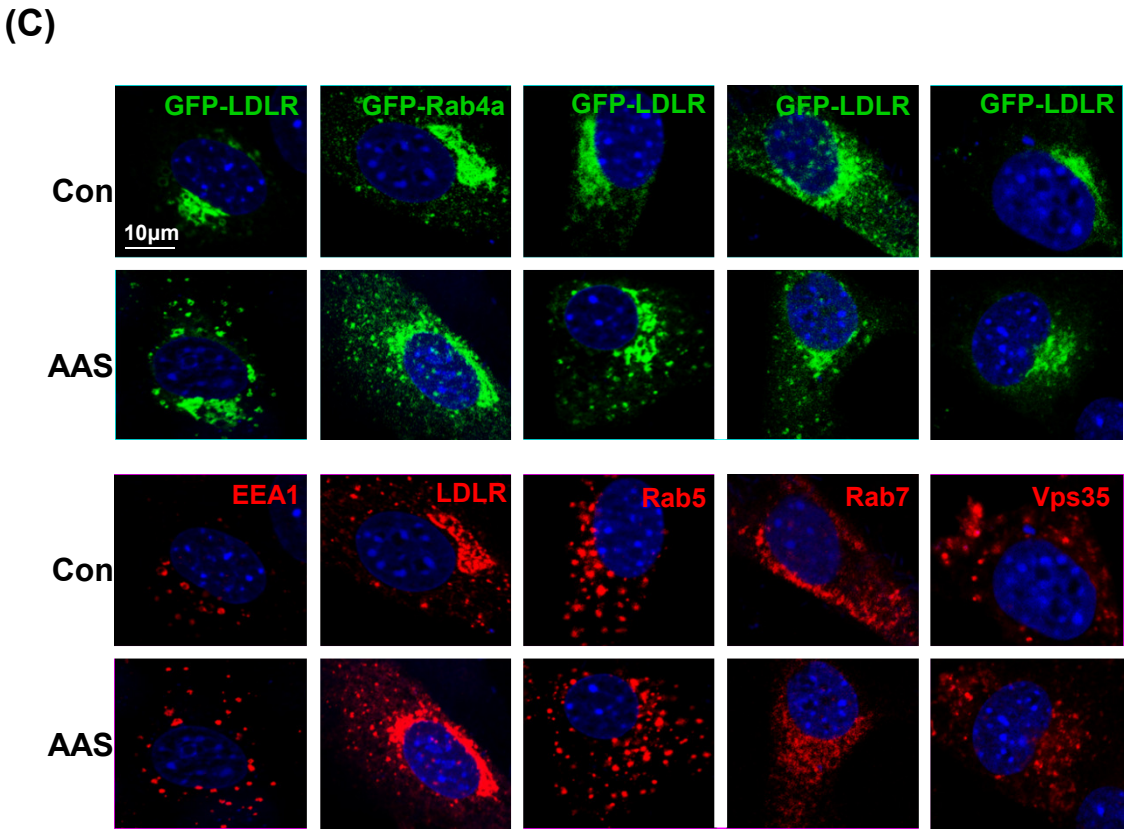

Appendix Figure S6 (part 2)

(D)

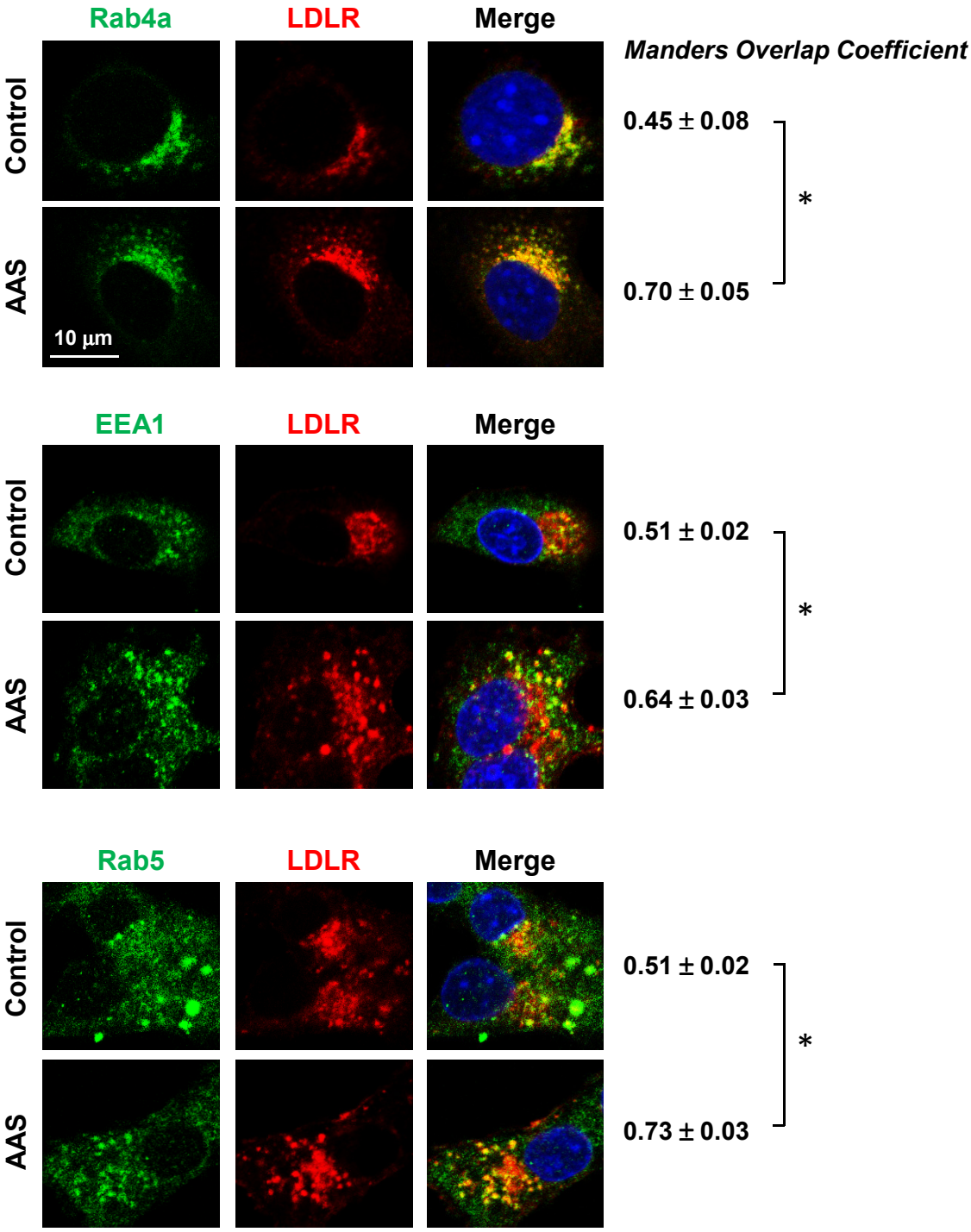

Data were mean ± SD. * *P* < 0.05, unpaired *t*-test (*n* = 4 - 5).

Appendix Figure S6 (part 3)

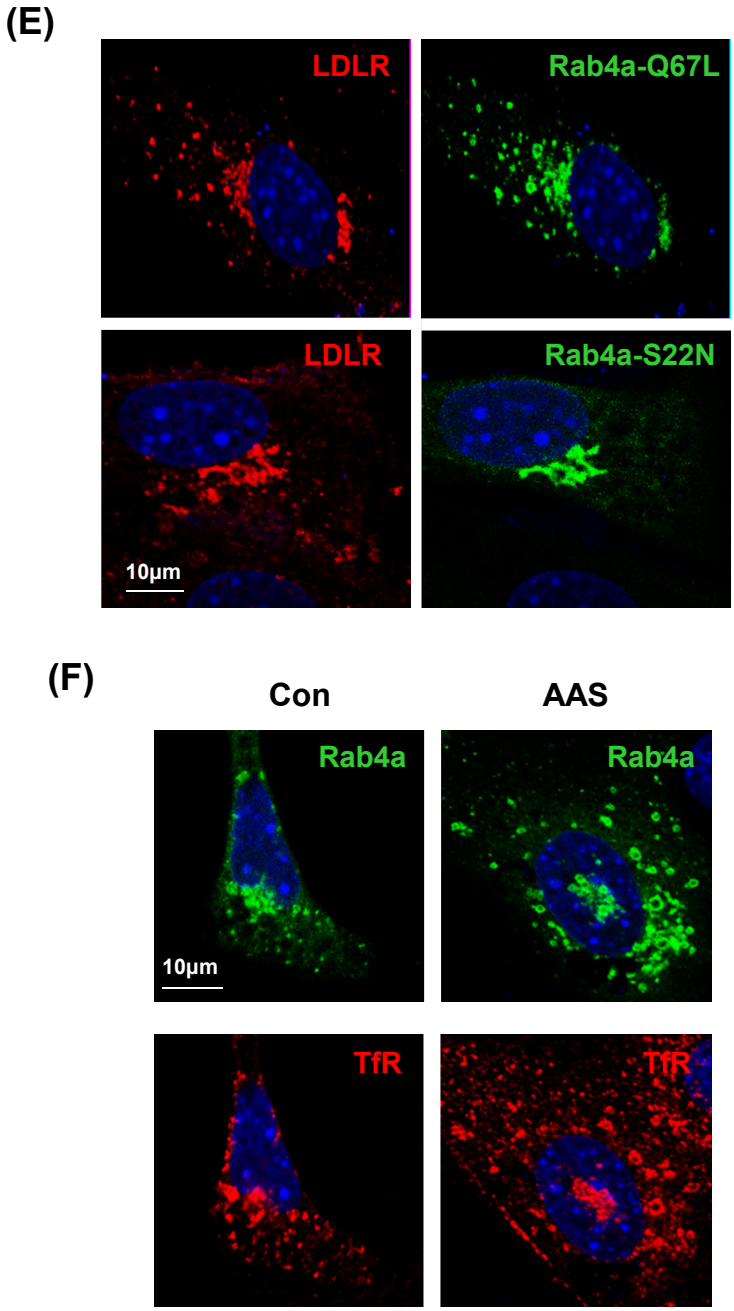

Figure S6. Effects of AAS on LDLR recycling. (A) Single color channel images for those in Figure 3B. (B) Original images of the fluorescence intensity profile data shown in Figure 3C, illustrating that AAS treatment increased the amount of LDLRs residing in vesicular structures away from the perinuclear center. White dotted arrows indicated the sampling location for fluorescence intensity profile analysis; red/green dotted lines marked the cell surface; blue dotted lines marked the nuclei. NB. The 2 images in the left panels were identical to those shown in Figure 3A. (C) Single color channel images for those in Figure 3D. (D) Double immuno-labeling of endogenous proteins showing that AAS increased LDLR co-localization with EEA1, Rab4a and Rab5, especially in the peripheral region of the cytosol. (E and F) Single color channel images for those in Figure 3H and 3I.

Appendix Figure S7

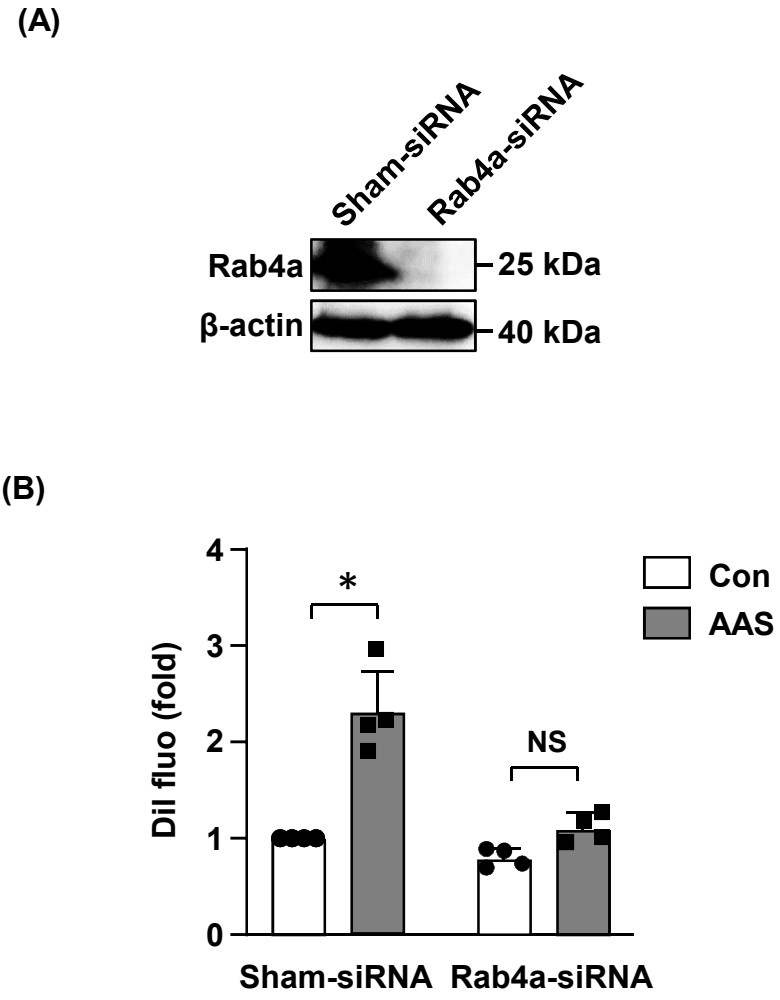

Figure S7. Effect of Rab4a gene silencing on AAS-induced LDL uptake in HepG2 cells. (A) Representative western blots showing the gene silencing efficacy of Rab4a siRNA transfection (example from 4 independent experiments). (B) Quantitative data of DiI fluorescence showing that Rab4a depletion diminished AAS (50%)-stimulated DiI-LDL endocytosis. Data were mean ± SD. * $P < 0.05$, one-way ANOVA. NS, no significance.

Appendix Figure S8

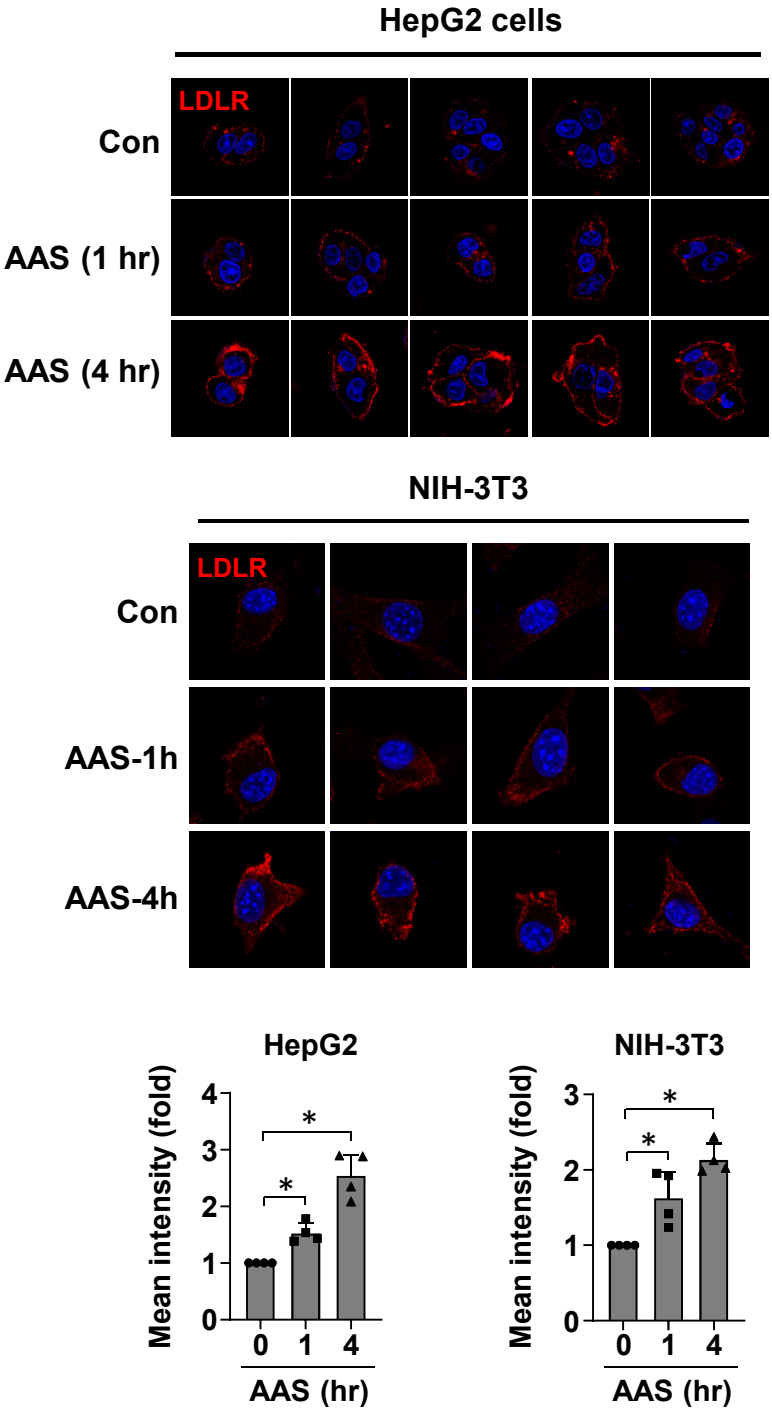

Figure S8. Representative confocal microscopy images and quantitative data (mean fluorescence intensity) showing that AAS (0%) significantly increased the abundance of LDLRs on the plasma membrane. Assays were performed in non-permeabilized cells. Numerical data were expressed as mean ± SD. * $P < 0.05$, one-way ANOVA.

Appendix Figure S9

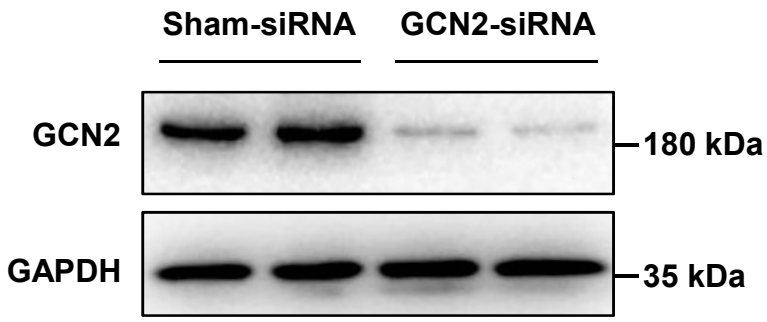

Figure S9. Representative western blots (example from 4 independent experiments) showing the gene silencing efficacy of GCN2 siRNA in HepG2 cells.

Appendix Figure S10

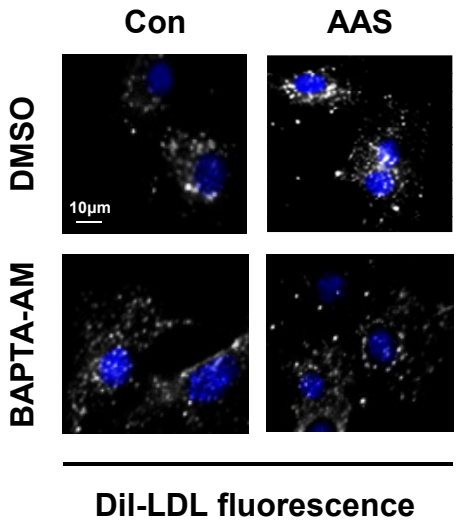

Figure S10. Representative fluorescence microscopy images showing that pre-incubation of NIH-3T3 cells with the membrane permeable Ca^{2+} chelator BAPTA-AM (5 µM) abolished AAS-induced endocytosis of DiI-LDL. DMSO was used as vehicle control. Cell nuclei were counterstained with DAPI (blue).

Appendix Figure S11

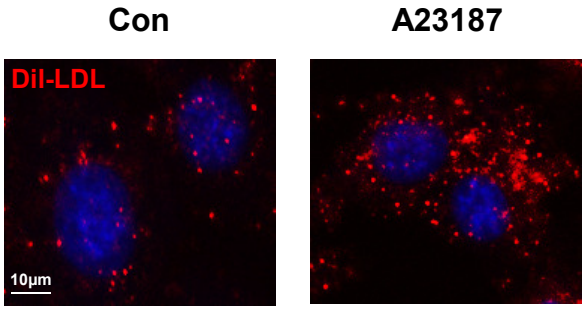

Figure S11. Representative fluorescence microscopy images showing that treatment of NIH-3T3 cells with the calcium ionophore A23187 (2 μM) accelerated DiI-LDL endocytosis. Cells were treated with A23187 for 120 min followed by incubation with DiI-LDL for 60 min. Cell nuclei were counterstained with DAPI (blue).

Appendix Figure S12

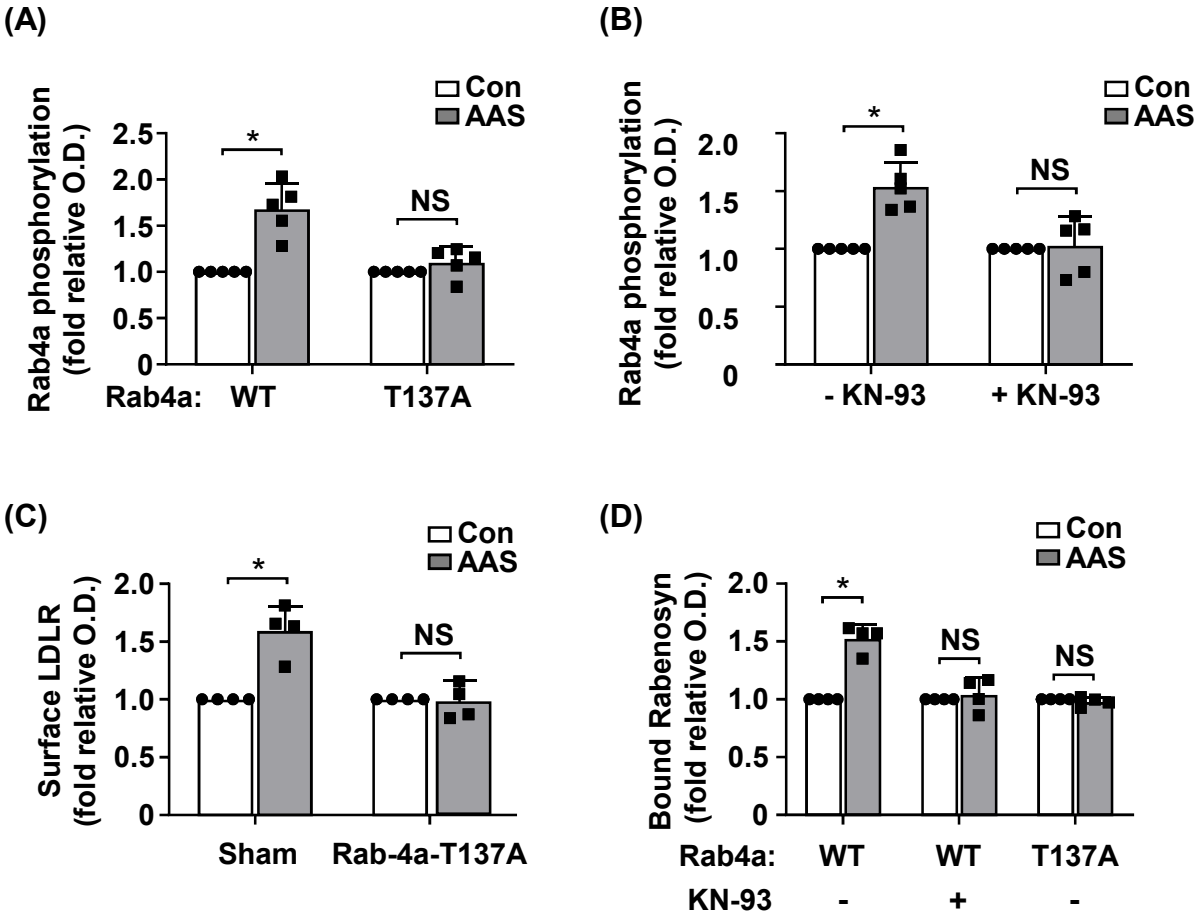

Figure S12. Quantitative densitometry data for western blot experiments shown in Figures 5E (A), 5F (B), 5H (C) and 5L (D). Data were expressed as mean ± SD. * $P < 0.05$, one-way ANOVA. NS, no significance.

Appendix Figure S13

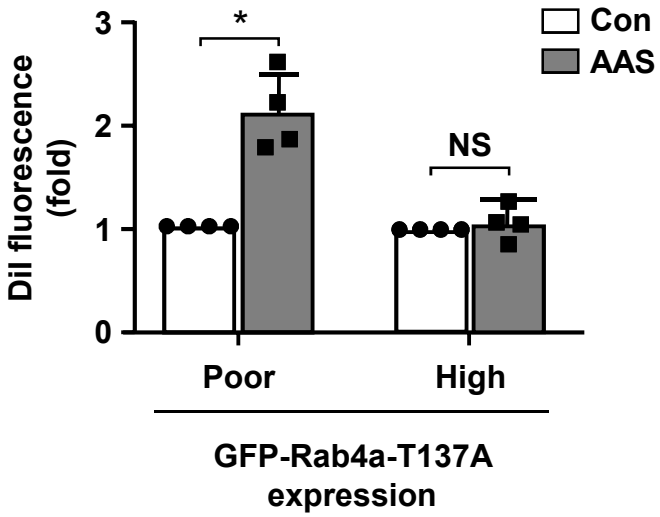

Figure S13. Quantitative fluorescence intensity data for experiments shown in Figure 5G, demonstrating that in NIH-3T3 cells with strong GFP-Rab4a-T137A expression, AAS failed to stimulate DiI-LDL endocytosis; in comparison, in cells with poor Rab4a-T137A expression, the responsiveness to AAS was retained. Data were expressed as mean ± SD. * $P < 0.05$, one-way ANOVA. NS, no significance.

Appendix Figure S14

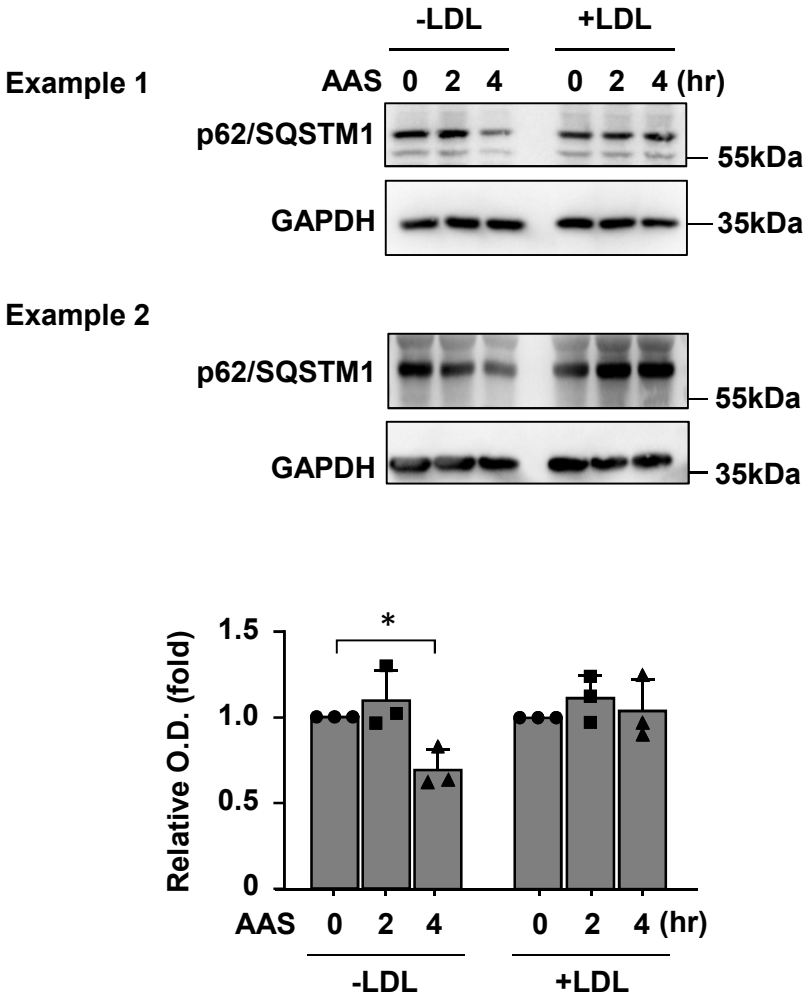

Figure S14. Two examples of western blot results and corresponding quantitative densitometry data showing that AAS-induced increase in autophagy (increase in LC3-II) in HepG2 cells (refer to Figure 7A) was not accompanied by accumulation of p62/SQSTM1, indicating that the effect of AAS was not due to blockade of the normal autophagic flux. Data were expressed as mean ± SD. * $P < 0.05$, one-way ANOVA.

Appendix Figure S15

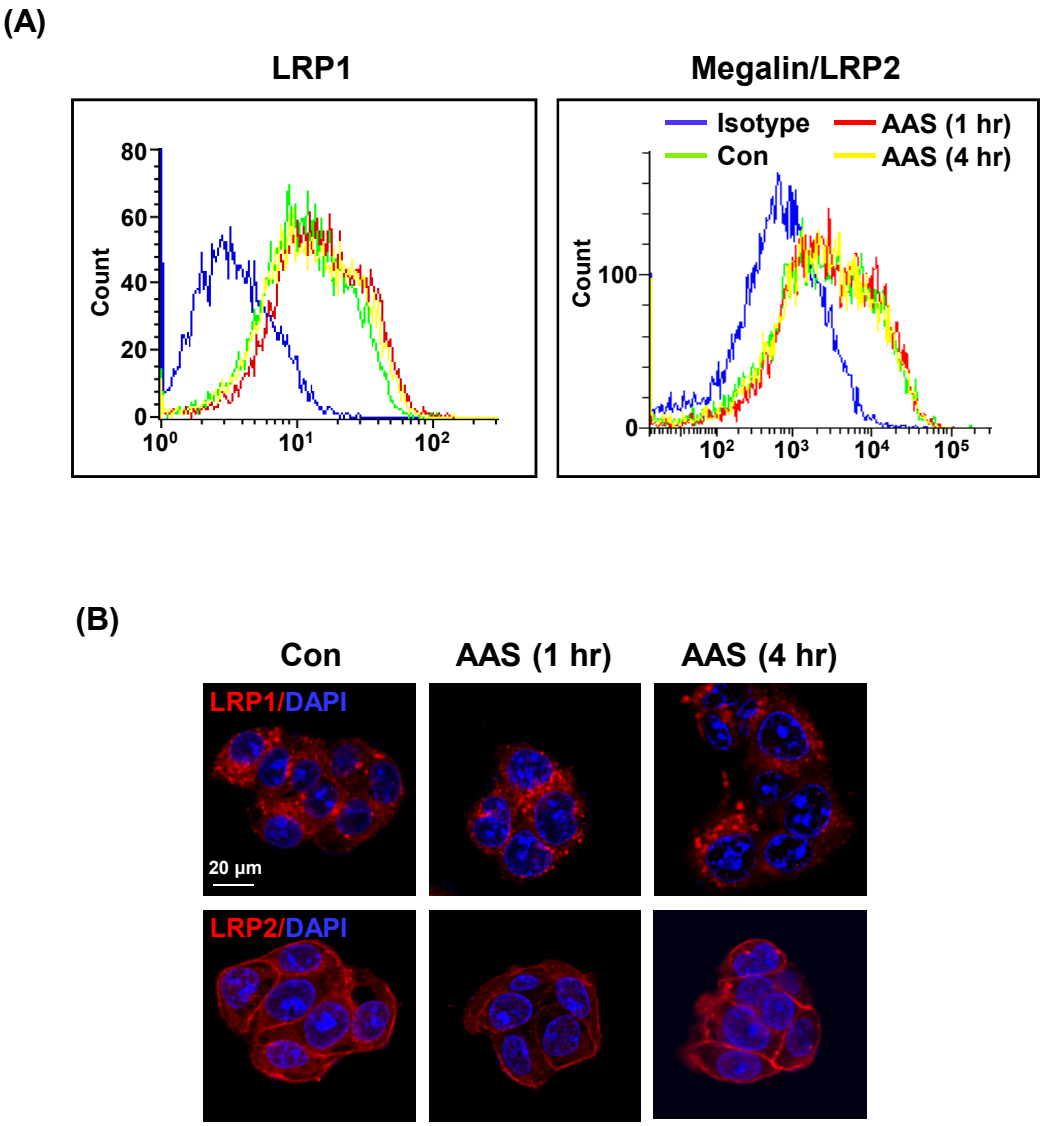

Figure S15. Representative results of (A) flow cytometry (from 3 independent experiments) and (B) confocal microscopy images of immunofluorescence (preliminary data from 2 independent experiments) showing that AAS (0%) stimulation did not increase the abundance of LRP1 or megalin/LRP2 on the cell surface. All assays were performed in non-permeabilized HepG2 cells. Specific labeling of plasma membrane located proteins by immunofluorescence was performed as described in the Materials and Methods section.

Appendix Table S1. Summary of the Manders Overlap Coefficient values for double immuno-labeling experiments

Data Sets	Treatment Groups	
Figure 3D	***Control***	***AAS***
LDLR/EEA1	0.51 ± 0.02	0.64 ± 0.03*
LDLR/Rab4a	0.48 ± 0.04	0.72 ± 0.04*
LDLR/Rab5	0.51 ± 0.02	0.73 ± 0.03*
LDLR/Rab7	0.48 ± 0.05	0.49 ± 0.05
LDLR/Vps35	0.53 ± 0.07	0.50 ± 0.03
Figure 3H		---
LDLR/Rab4a-Q67L	0.70 ± 0.08	---
LDLR/Rab4a-S22N	0.44 ± 0.11	---
Figure 3I		
TfR/Rab4a	0.62 ± 0.07	0.63 ± 0.07
Figure 4H	***Control***	***A23187***
LDLR/Rab4a	0.45 ± 0.08	0.73 ± 0.04*
Figure 5K	***Control***	***Okadaic acid***
LDLR/Rab4a	0.46 ± 0.06	0.70 ± 0.04*

Data were mean ± SD. * $P < 0.05$ versus control, unpaired *t*-test ($n = 3$ - 5).

Appendix Table S2. Primer and siRNA sequences used in the study

siRNA constructs	***Forward***	***Reverse***
Atg5 (human)	CCAUCAAUCGGAAACUCAUTT	AUGAGUUUCCGAUUGAUGGTT
GCN2 (human)	CACCUACCUAUCCAGAUGUTT	ACAUCUGGAUAGGUAGGUGTT
Rab4a (human)	GGAGUGGAAUUUGGUUCAATT	UUGAACCAAAUUCCACUCCTT
COMMD1 (human)	GCUGGAAUUAGGCAAAUAUTT	AUAUUUGCCUAAUUCCAGCTT
WASH1 (human)	GUCCCAGAGAACUACUUCUTT	AGAAGUAGUUCUCUGGGACTT
Primers	***Forward***	***Reverse***
LDLR (Mouse)	CATCCTCGGACATCCACCC	TTCGGTCGTGGCACAAGAAC
LDLR (human)	ATGAGAAGAAGCCCAGTAGCG	CAAAGGAAGACGAGGAGCACGAT
Beclin-1 (human)	AACCGCAAGATAGTGGCAGA	CTCTCTGATACTGAGCTTCCTCC
Atg5 (human)	TCTGCTATTGATCCTGAAGATGGG	TCAATCTGTTGGCTGTGGGA
Atg7 (human)	CGCAGAGATGTGGAGCAACT	AGCTCCTTGCTGCTTTGGTT
LC3B (human)	CAGCATCCAACCAAAATCCCG	TTGAGCTGTAAGCGCCTTCTAAT
LDLR (for genotyping)	CTCCCAGGATGACTTCCGAT	CGCAGTGCTCCTCATCTGAC